O B S E R V A T I O N A L S T U D I E S

OF THE PLANETARY BOUNDARY LAYER

OVER LAND

B Y

S. J. C A U G H E Y

METEOROLOGICAL RESEARCH UNIT
RAF CARDINGTON
BEDFORD

UNITED KINGDOM

1. Introduction

The past decade has seen rapid advances in our understanding of the structure of turbulence in the atmospheric surface layer, both in convective and stable conditions. However it is still fair to say that relatively little information exists on the rather inaccessible regions above the surface layer, more especially those above the reach of tall towers. To meet this need the Boundary Layer Branch of the British Meteorological Office has developed, over the course of the last twenty years, instrument packages suitable for mounting on the tethering cable of large (1300 m^3) balloons and capable of making accurate, fast response , measurements of the turbulent flow for periods of up to 24 hours at heights up to about 2 km.

The present version of the turbulence probe consists essentially of a set of sensors mounted on a vane which is attached to the balloon tethering cable in a way that leaves it free to rotate and thus keep the sensors facing into wind. The temperature (T) sensor consists of 180 cm, 26-μ diameter platinum wire wound non-inductively on a plastic former. A double V-shaped hot wire inclinometer mounted on a damped pendulum measures the inclination (ϕ) of the wind to the horizon while a second inclinometer, orientated at 90° to the first, measures the instantaneous horizontal wind direction (θ), relative to the vane direction. A magnetic flux valve is used to sense the vane direction (D), relative to the earth's magnetic field. Wind speed (V) is measured with a multislot photo-electric anemometer fitted with an eight-cup polystyrene rotor. From the four basic quantities i.e. ϕ, V, θ , and D the three orthogonal wind components (U,V, and W) are derived. Some of the supporting electronics is housed in the fin of the vane and the remainder in a box (which also contains the power supply) attached to the cable a short distance below the probe. All signals are relayed to the ground by radio telemetry and recorded on magnetic tape.

A series of evaluation experiments have been carried out jointly with AFCRL using their sonic instrumentation as a standard. Side by side comparisons on fixed supports showed excellent agreement between the average statistics from the two systems. In order to assess the significance of balloon/cable movement effects the MRH probes were flown at 300 and 150 m on the balloon whilst the AFCRL sensors were positioned at the same heights on a tall tower. These results are discussed in detail by Haugen et.al. (1975) and show that the vertical velocity and temperature measurements are negligibly affected by balloon movement whereas the horizontal wind components are somewhat overestimated (10 - 20 %) (Figs. 1 and 2).

During the last six or seven years the instrumentation has yielded much useful information on the higher regions of the boundary layer and in this talk I can do little more than describe a selection of the results obtained. Early work consisted of raising a single package through the depth of the convective boundary layer with short duration stops at standard levels. These studies yielded useful results on the behaviour of the vertical profiles of the rates of dissipation of turbulent kinetic energy (ε) and temperature variance (N) (Caughey and Rayment, 1974). In cases with strong convective mixing ε showed little decrease with height whereas in neutral conditions a marked decrease with height was observed . On the other hand N was found to decrease rapidly with height at all times.

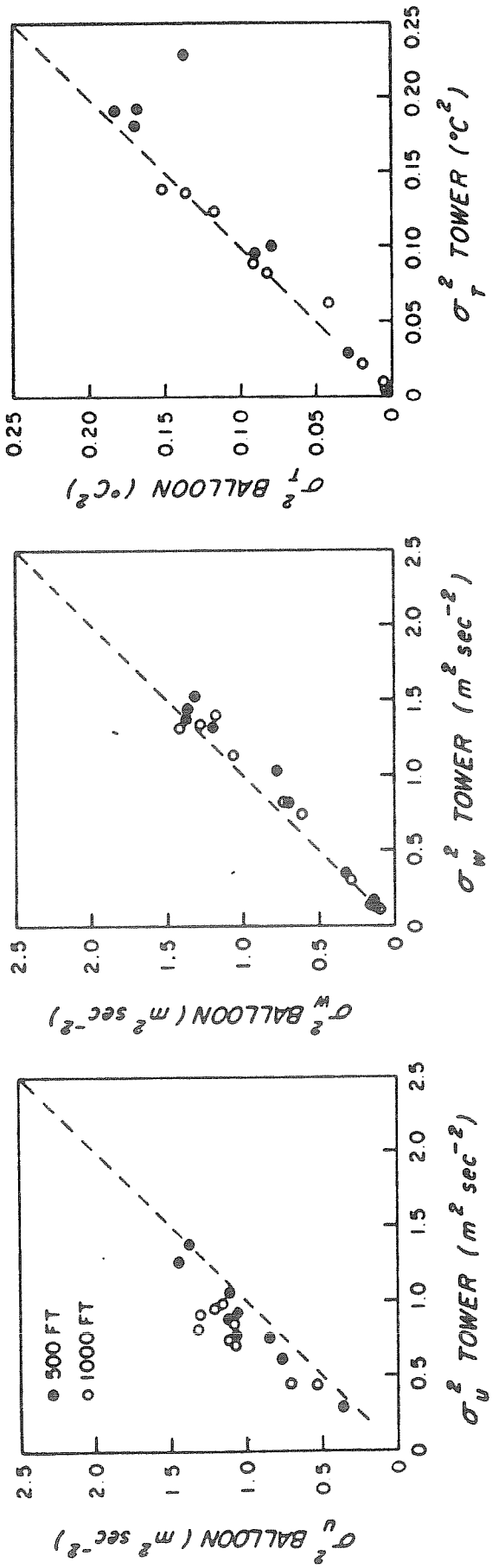

Figure 1: Comparison of variances from balloon-borne (MRU) and tower based probes (AFCRL).

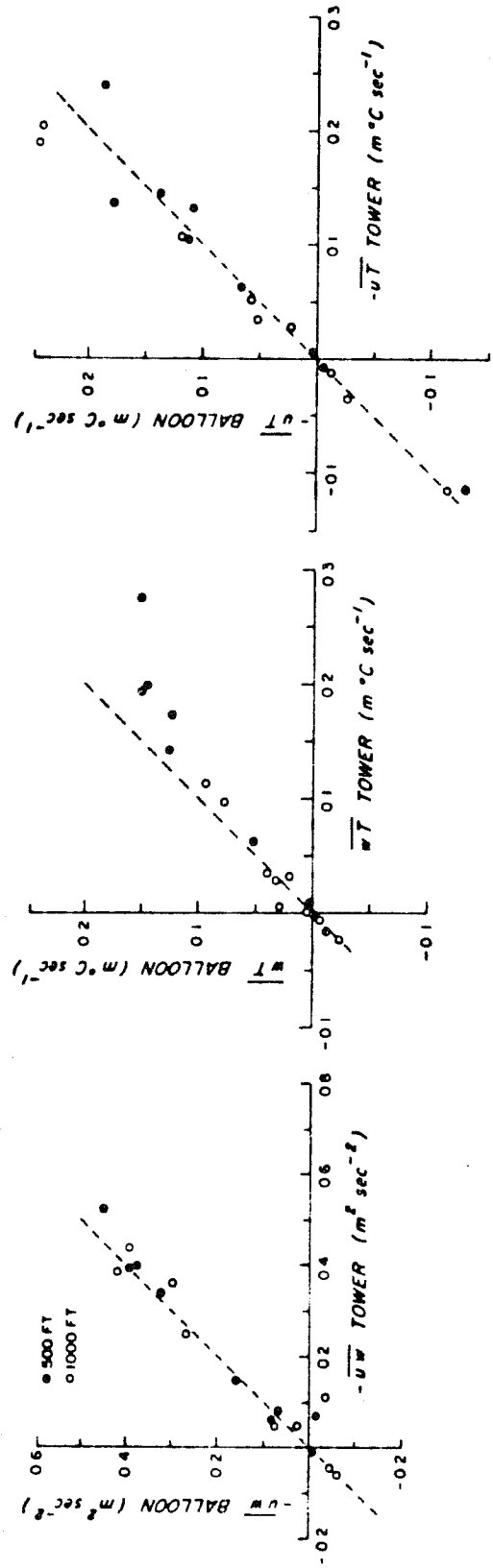

Figure 2: Comparison of covariances from balloon-borne (MRU) and tower based probes (AFCRL).

2. Convective conditions - the Minnesota Boundary Layer Experiment

In the autumn of 1973 a full-scale boundary layer experiment was carried out jointly with AFCRL in a sparsely populated region of northwestern Minnesota (Kaimal et. al. 1976). The AFCRL instrumentation was mounted at standard levels on a 32 m tower and the MRU turbulence probes at heights of 61, 152, 305, 610 and 1200 m on the balloon cable. During periods of data gathering the actual heights of the probes were measured periodically with a double theodolite system. The observational periods included in this data set fall within the time interval 1200 to 1800 CDT when the height of the lowest inversion base was roughly constant and the surface heat flux directed upwards. The common averaging period for all data is 75 min. A detailed discussion of data reduction procedures is given by Izumi and Caughey (1976).

In midlatitudes over land the convective boundary layer typically reaches a height of 1 to 2 km by mid-afternoon, and is often capped by an inversion. This layer exhibits a near-constant distribution of wind speed and potential temperature, obviously a consequence of the strong vertical mixing produced by convection. The name ' mixed layer ' is thus often used synonymously with the convective boundary layer.

Illustrated in Figure (3) are the wind speed and temperature profiles for run 2A1 and these are fairly typical of daytime convective conditions. Almost all the wind shear and all the potential temperature gradient in the boundary layer are confined to a very shallow region close to the ground. The boundary layer over land may be idealized as a three layer structure in terms of the parameters considered relevant to the turbulence in each.

Proceeding upward from the surface,

a. The surface shear layer where wind shear plays a dominant role. Here Monin-Obukhov similarity applies and the controlling parameters are z, τ_o, Q_o and g/T . The scaling velocity and temperature for this layer are, respectively :

$$U_* = (\tau_o/\rho)^{\frac{1}{2}} \qquad (1)$$

$$T_* = -(Q_o/u_*)$$

The expectation is that dimensionless groups formed with U_* and T_* become universal functions of Z/L. Widespread support for these ideas (with the exception of the U and V statistics) can be found in the literature (Businger et.al. 1971, Wyngaard and Coté 1971, Kaimal et. al. 1972, Busch 1973, Caughey and Readings 1974, 1975). The shear layer is confined to a height $z \leq -L$.

b. The free convection layer where τ_o is no longer important but height, Z, continues to be the significant length scale. The governing parameters reduce to three: z , Q_o and g/T which yield a scaling velocity, U_f , and scaling temperature, T_f , given by

$$U_f = [Q_o z (g/T)]^{1/3} \qquad (2)$$

$$T_f = [Q_o / u_f]$$

According to the local free convection predictions of Wyngaard et. al. (1971)

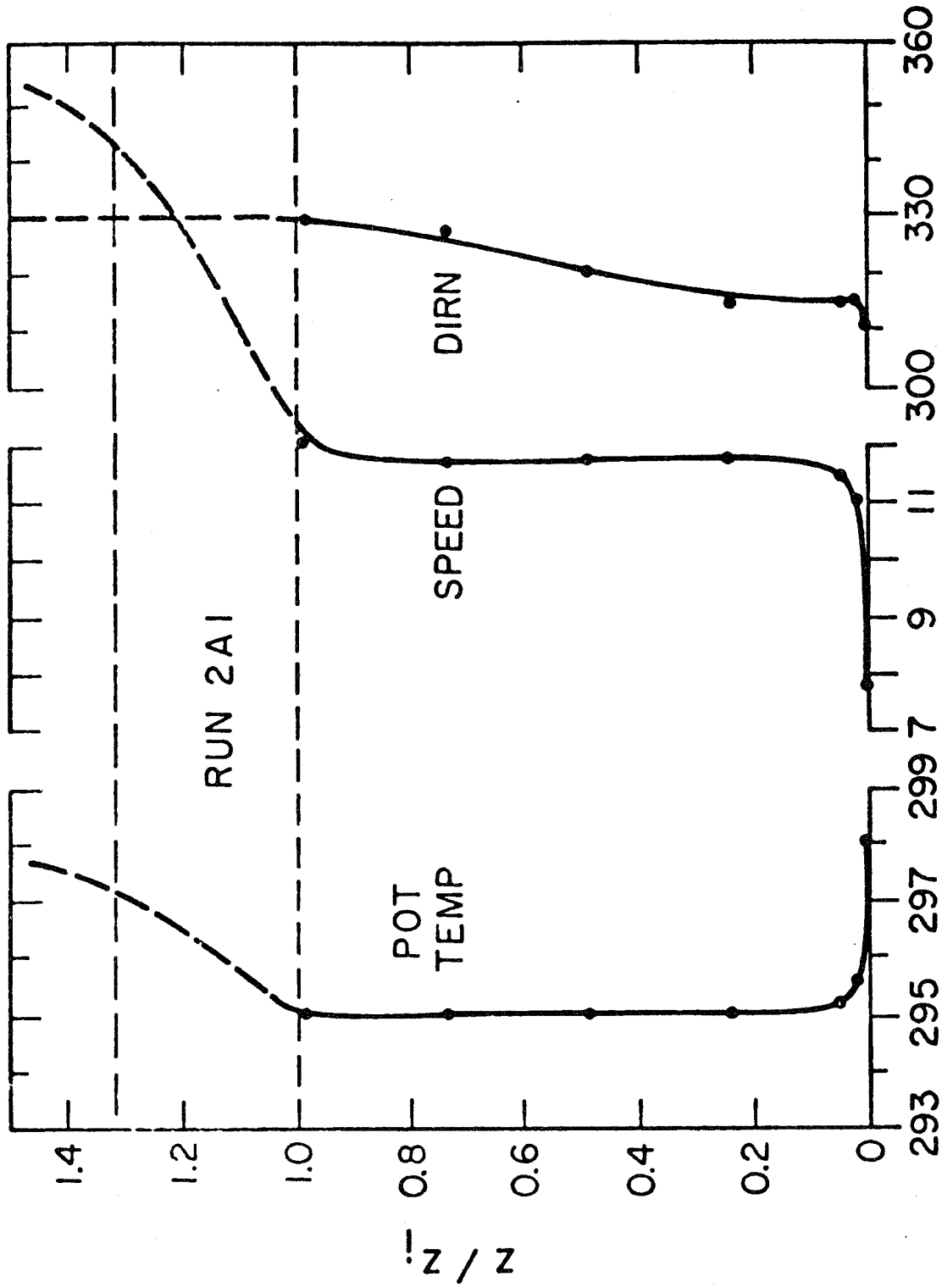

Figure 3: Profiles of wind speed, wind direction and temperature for Run 2A1. The near adiabatic lapse rate and the negligible mean wind shear in the mixed layer is typical for observational periods comprising this data set.

dimensional groups formed with U_f , T_f should be constants. The very unstable ($-Z/L > 1$) data from Kansas support these predictions in the main. Our present data set suggests an upper limit of approximately 0.1 Z_i for this layer.

c. The mixed layer in which the structure of turbulence is insensitive to Z as well as τ_o. The thickness of the boundary layer, defined as the height of the lowest inversion base Z_i, is taken to be the controlling length scale, so that the scaling velocity and temperature for this layer become

$$W_* = \left[Q_o Z_i \, g/T\right]^{1/3}$$

$$\theta_* = Q_o / W_* \qquad (3)$$

Within this region dimensionless groups formed with W_* and θ_* should be functions only of Z/Z_i. This expectation is based on model studies (Deardorff 1972, Wyngaard et. al. , 1974) which show wind and temperature data scaling with W_* and θ_* . The Minnesota data will be presented within this framework of mixed layer similarity.

Controversy still exists regarding the choice of Z_i for the thickness of the convective boundary layer and it is worth noting that the Minnesota data set does not add much further support for the usefulness of Z_i as a boundary layer length scale. This arises primarily because of the small variation in Z_i between the various days (a factor of two) and the important processes not accounted for in the presently used mixed layer similarity theory e.g. entrainment, baroclinicity etc., which are presumably contributing to the scatter in the data points. In this respect the removal of Z_i from many of the mixed-layer similarity plots does not significantly increase the scatter. Some investigators (Tennekes,1970, Zilitinkevich,1972, Clarke and Hess, 1973) have suggested that this thickness is a function of U_*/f , the Ekman layer depth. However, the modelling studies of Deardorff (1974a) show that Z_i the height of the lowest inversion base determines the boundary layer depth. He found the heights of the boundary layer for both heat and momentum to be nearly the same and approximated by Z_i.

Estimating Z_i presented no difficulty in these observations as the base of the capping inversion was sharply defined in all the radiosonde ascents. Between sunrise and noon Z_i grew rapidly in response to the steadily increasing surface heat flux. The growth of Z_i slowed down between 1300 and 1600 CDT as Q_o reached its maximum value. As Q_o decreased through the late afternoon Z_i began to level off to a nearly constant value which it maintained even after Q_o turned negative (see Fig. 4).

2.1 Spectra of Velocity Components:-

Atmospheric surface layer spectra and cospectra ,when expressed in appropriate similarity coordinates, reduce to a set of universal curves that converge into a single curve in the inertial subrange, but spread out as a function of Z/L at lower frequencies (Kaimal et.al. 1972). It is of interest to see whether the spectral properties of the convective boundary layer can similarly be generalized through proper normalization of the spectral intensities and frequency scales.

Two facts emerged from an examination of velocity spectra obtained from the mixed layer. The energy in the inertial subrange remains essentially constant with height (in contrast with the sharp decrease with Z observed near the ground) and the spectral peaks tend to be invariant both in their intensities and their positions on the frequency scale. These observations imply near uniform spectral behaviour over much of the boundary layer, so the use of mixed layer scaling appears logical. Extending the similarity argument to the mixed layer, we can expect the velocity spectrum normalized by W_*^2 to be a function of only two variables, Z/Z_i and

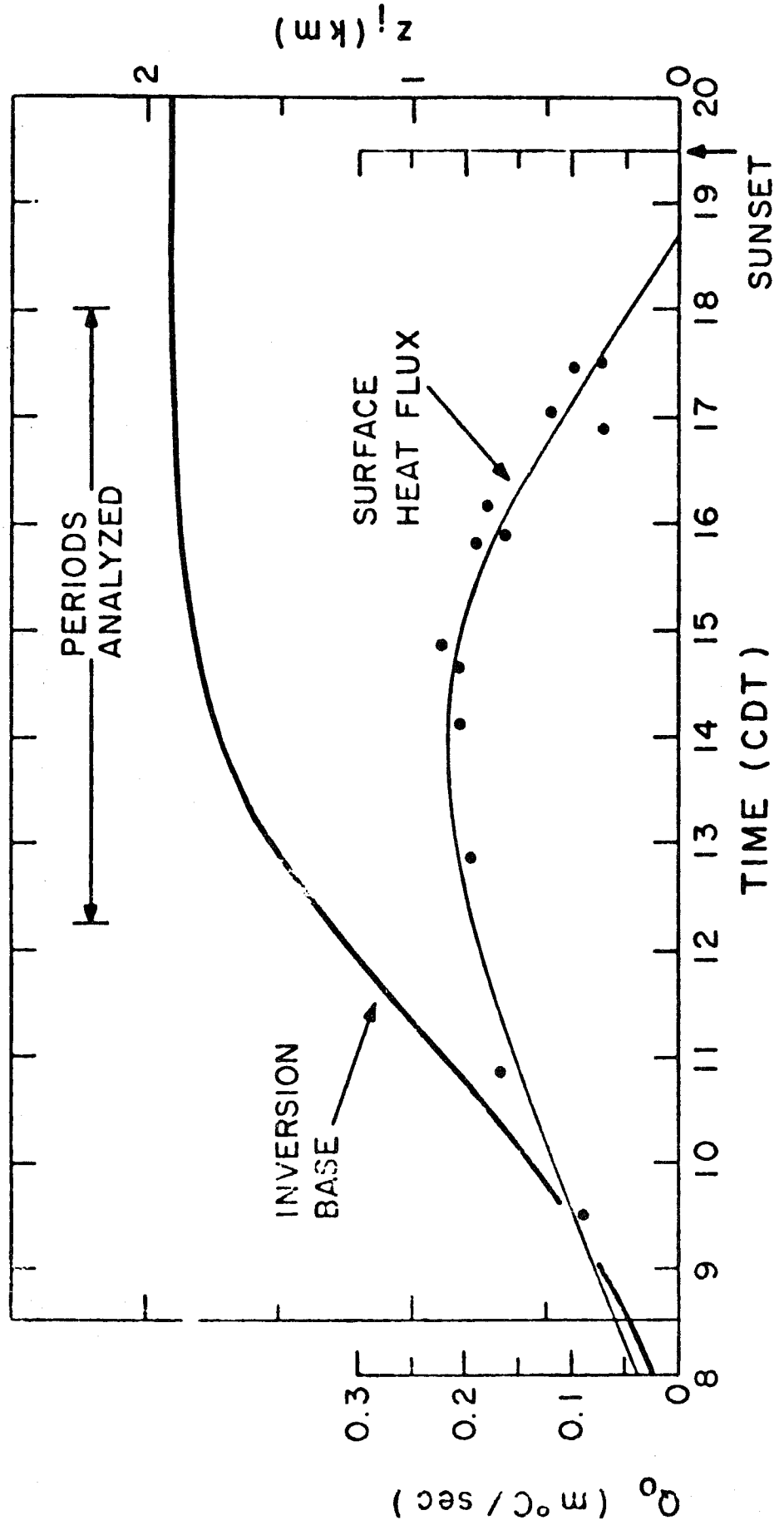

Figure 4: Diurnal trend in the surface heat flux and corresponding inversion rise for a typical day.

λ/z_i (where λ is the wavelength approximated by $\bar{u}/n$). Thus, the one-dimensional logarithmic U spectrum can be expressed as

$$\frac{n S_u(n)}{w_*^2} = \frac{\alpha_1}{(2\pi)^{2/3}} \psi^{2/3} f_i^{-2/3} \qquad (4)$$

where α_1 is the spectral constant for U, ψ is the dimensionless dissipation rate $\left(\frac{\varepsilon T}{\rho \Omega_0}\right)$ appropriate to the mixed layer and f_i is the dimensionless frequency $\left(\frac{nz_i}{\bar{u}}\right)$ for that layer. By our similarity argument, ψ, the ratio of local kinetic energy dissipation to buoyancy production at the surface should be a universal function of z/z_i and there is strong evidence from the Minnesota data in support of this contention. Taking $\alpha_1 = .5$ and rearranging terms Eq (4) becomes

$$\frac{n S_u(n)}{w_*^2 \psi^{2/3}} = 0.15 f_i^{-2/3} \qquad (5)$$

Spectral forms for the one-dimensional V and W spectra differ from Eq (5) by a factor of 4/3 as a consequence of isotropy, so that

$$\frac{n S_v(n)}{w_*^2 \psi^{2/3}} = \frac{n S_w(n)}{w_*^2 \psi^{2/3}} = 0.20 f_i^{-2/3} \qquad (6)$$

Logarithmic spectra normalized in this manner show systematic behaviour when plotted as a function of f_i (see Fig. 5). Inclusion of $\psi^{2/3}$ in the normalization forces all spectra to collapse into a single curve in the inertial subrange. At lower frequencies we find the curves separating as a function of z/z_i. However the separation is not nearly so systematic as in the Kansas spectra but the demarcation between categories is, nevertheless, clear enough to justify the curves in Fig. (5). The spectra used for constructing the composite plots were subjected to minor smoothing by eye to remove the distortions introduced by balloon movement at the high frequency end.

Of the three velocity components W shows the largest spread with height. The normalization tends to exaggerate the spread in the ordinate but the separation in the abscissa is expected since the length scales of W are known to be strongly height dependent in the lower layers of the atmosphere. As z/z_i increases from 0.01 to 1.0 the spectral peak shifts to lower values of f_i, rather rapidly at first up to $z/z_i = 0.1$ then more gradually above that. For U and V only two categories exist: 0.01 to 0.02 + 0.02 to 1.0 and the shift in the spectral peak is virtually insignificant.

The dimensionless dissipation rate, ψ, which appears in the normalization of the spectral intensities, assumes a nearly constant value in the mixed layer, falling between 0.5 and 0.7 . The limiting wavelength for the inertial subrange appears to be a function of z_i in the mixed layer. Based on Fig. (5) we can define the limit as $\lambda \leq 0.1\, z_i$. In the surface layer this limiting wavelength is approximately the height above the ground (Kaimal et.al. 1972) so we have to assume the transition from the z to z_i dependence occurs within the height range 0.01 to 0.1 z_i.

The peak wavelength, λ_m, in the W component also undergoes a similar transition with height. This wavelength is important for studies of turbulent transport in the boundary layer and therefore merits close examination. In Fig. (6) we have λ_m normalised with z_i plotted as a function of z/z_i. At $z \leq 0.1\, z_i$ the relationship is a linear one,

$$\frac{\lambda_m}{z_i} = 5.9 \frac{z}{z_i}$$

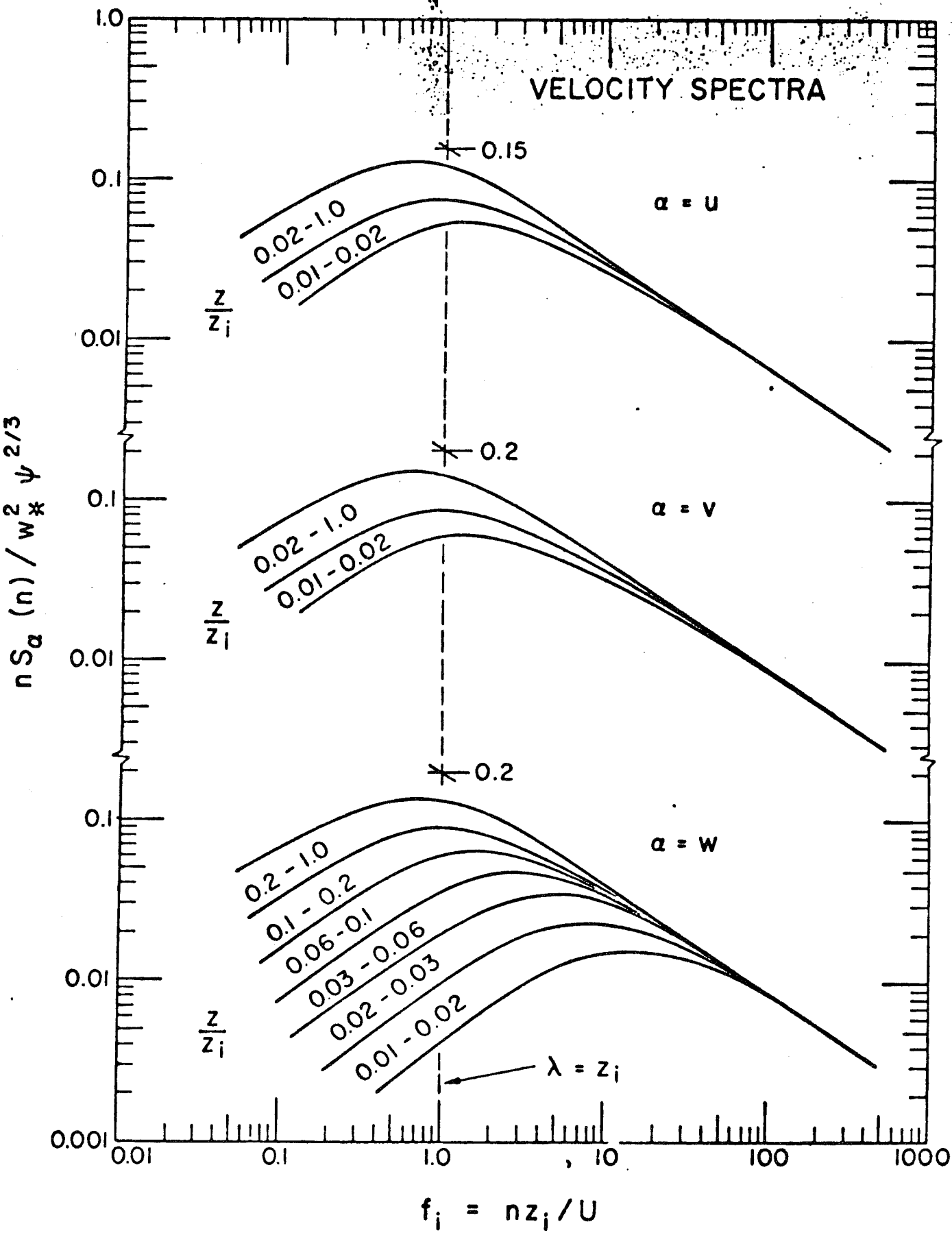

Fig. 5: Universal curves for velocity spectra expressed in mixed layer similarity coordinates. The function ψ in the spectral normalisation is the dimensionless energy dissipation rate ($\varepsilon T/gQ_o$).

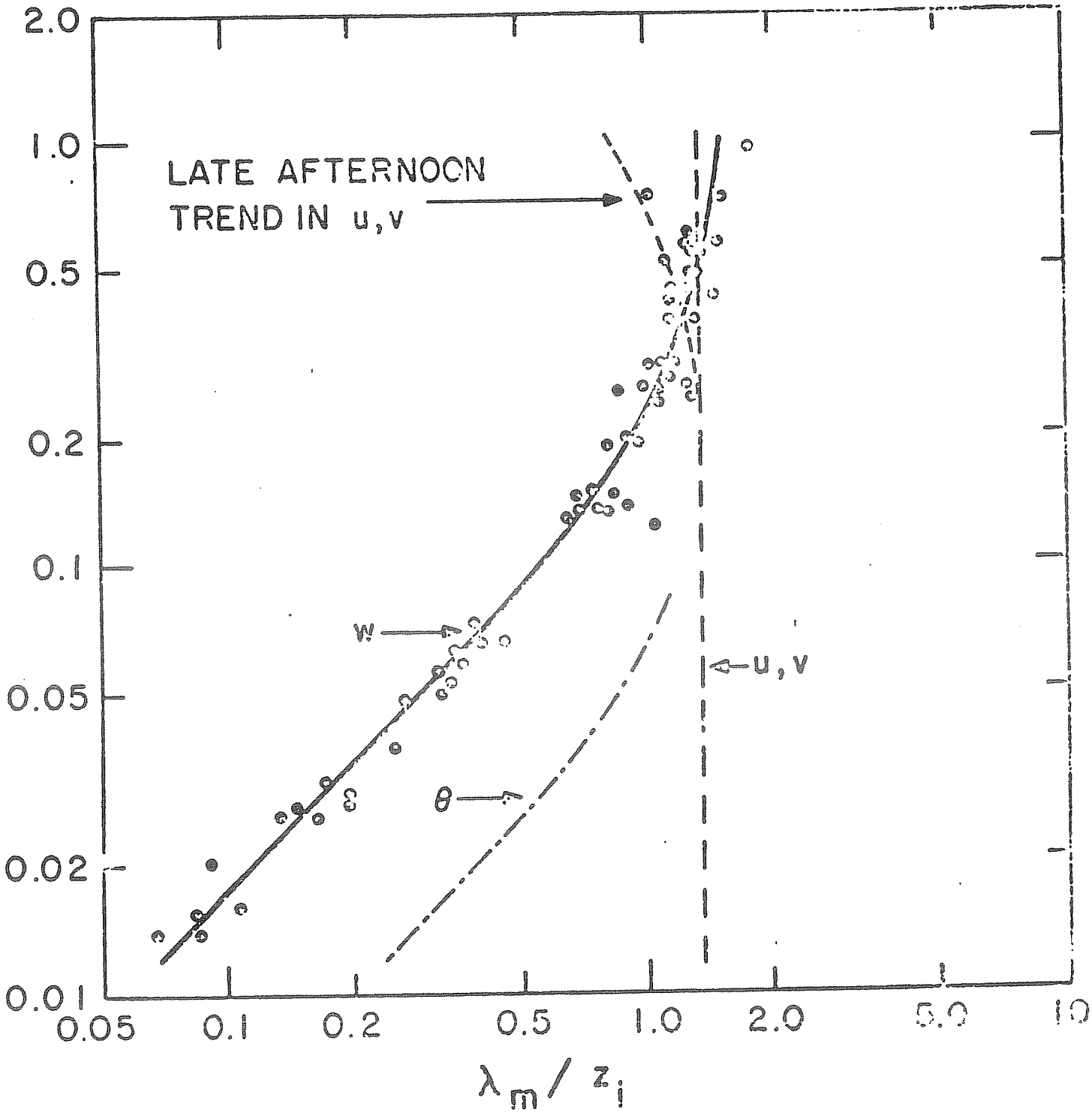

Fig. 6: Dimensionless peak wavelength for the velocity components and temperature plotted as a function of Z/Z_i. Scatter in the U, V and θ data points (not shown) is about twice as large as for W.

which is precisely the free-convection limit $\frac{\lambda_m}{z} = (\cdot 17)^{-1}$ observed in the Kansas data (Kaimal et.al. 1972). Above 0.1 z_i, λ_m increases more gradually and finally approaches a constant value ($\sim 1.5\ z_i$) in the range 0.5 z_i - z_i. An exponential relationship for its behaviour above 0.1 z_i has been suggested by D H Lenschow (personal communication) whose aircraft W spectra show similar behaviour. Combining the Kansas and Minnesota results we can approximate λ_m for W in different regions of the convective boundary layer as follows

$$(\lambda_m)_w = \begin{cases} z/(0.55 - 0.38\, z/|L|)\ ; & 0 \le z \le -L \\ 1.8\, z & ;\ -L \le z \le 0.1 z_i \\ 1.8\, z_i [1 - \exp(-5z/z_i)]\ ; & 0.1 z_i \le z \le z_i \end{cases} \qquad (7)$$

For U and V components, λ_m/z_i shows little, if any, variation with z/z_i. The scatter in the data (not shown in this plot) is larger than for W, by at least a factor of 2. But their average value 1.3, shown by the dashed line came close to the asymptotic limit of 1.5 for W. Thus, in the mixed layer, we see a strong tendency for the wavelength in all components to be the same and roughly equal to 1.5 times the boundary layer thickness.

These observations are in general accord with those reported by other investigators. Deardorff's (1974b) numerical experiments showed λ_m/z_i, for the W spectra to be approximately 1.0 for z/z_i between 0.38 and 0.69. The aircraft measurements of Kukharets (1974) showed λ_m for W increasing with height between 50 and 500 m and approaching a constant value above 500 m. He also found λ_m sensitive to changes in terrain type (steppe, desert and ocean) which might possibly be the response to changes in z_i. In the surface layer it had been found that U and V do not obey Monin-Obukhov similarity under unstable conditions. The absence of any systematic variation with Z/L indicated that some length scale other than Z and L controls the behaviour of λ_m. It appears from the Minnesota data that this controlling length scale is of the order of z_i.

The observed λ_m matches the horizontal length scale of large convective plumes or thermals which extend through the depth of the boundary layer. The existence of organised convection on this scale has been observed by other investigators: Hardy and Ottersten (1969) and Konrad (1970) with the help of high-powered radars, Rowland and Arnold (1975) with FM-CW radar and Frisch et. al. (1975) with a combination of dual Doppler radar, acoustic sounder and microbarograph array. In the Minnesota data evidence of such structures can be found in the temperature records from heights above 0.1 z_i. The traces show positive bursts spaced 4 to 5 minutes apart, i.e. the time scale represented by λ_m in the mixed layer. The records show a high degree of correlation between these fluctuations and the fluctuations in the velocity field responsible for the peaks in Fig. (5) ,which suggest that the length scales of three-dimensional turbulence in the boundary layer are determined primarily by the convection pattern. In the U and V components these long-period fluctuations can be observed down to very small heights above the ground.

2.2 Spectrum of Temperature

The spectrum of temperature, unlike velocity spectra, cannot be conveniently generalized within the framework of mixed layer similarity. The difficulty arises mainly from run-to-run variations in the low frequency variance introduced by entrainment effects in the upper half of the boundary layer. However some useful generalizations can be made about spectral shape and inertial subrange intensities in the convective boundary layer.

These are contained in the set of indealized spectral curves shown in the lower plot of Fig. (7). At the low frequency end they all converge to a single curve which extends upward, reflecting the diurnal trend in temperature. At inertial subrange frequencies the spectral intensity drops steadily with height up to 0.5 Z_i, stays at a low value between 0.5 and 0.7 Z_i and starts to rise again above 0.7 Z_i. The leveling off and subsequent increase in the spectral level in the upper regions of the boundary layer clearly reflect the mixing produced by the entrainment of warm air through the capping inversion.

The only region in which generalization is possible is in the height range $Z \leq 0.1 Z_i$ where the θ spectra behave much like those obtained in the Kansas experiment (Kaimal et.al.1972). The controlling length scale here is Z not Z_i, therefore we use f for the dimensionless frequency scale.

The logarithmic one-dimensional θ spectrum for the inertial subrange can be expressed in the form (Kaimal et.al.1972)

$$n S_\theta(n) = \frac{\beta_1}{(2\pi)^{2/3}} N \varepsilon^{-1/3} Z^{2/3} f^{-4/3} \qquad (8)$$

where β_1, is the spectral constant for θ, assumed to be 0.8 (from Kansas results), and N is the dissipation rate of θ^2/Z. Substituting the value for β_1, normalising the spectral intensity with T_f^2, where T_f is the free-convection scaling temperature, and rearranging terms, we have

$$\frac{n S_\theta(n)}{T_f^2 \gamma} = 0.24 f^{-2/3} \; , \; \gamma = \frac{N \varepsilon^{-1/3}}{Q_0^{4/3} (g/T)^{-2/3} Z^{-4/3}} \; . \qquad (9)$$

This normalisation brings all θ spectra into coincidence in the inertial subrange as seen in the upper plot of Fig (7). At mid and low frequencies they collapse into a fairly narrow band with no clear tendency to separate according to Z/Z_i. λ_m for this composite spectrum approximates 20Z, the free convection limit in the Kansas spectra. As Z approaches 0.1 Z_i we see λ_m approaching the characteristic wavelength 1.5 Z_i, found in the velocity components. Above .1 Z_i, λ_m shows a tendency to increase a little with height up to 0.5 Z_i and to decrease again above 0.7 Z_i.

The function γ is essentially a dimensionless form of the structure parameter, C_T^2. We can write,

$$C_T^2 = 4 \beta_1 N \varepsilon^{-1/3} \simeq 3.2 N \varepsilon^{-1/3} \qquad (10)$$

The Kansas data provide the relationship between C_T^2 and surface layer parameters for local free convection (Wyngaard et.al. 1971).

$$C_T^2 = 2.67 Q_0^{4/3} (g/T)^{-2/3} Z^{-4/3} \qquad (11)$$

From (10) and (11) combined with (9) we have $\gamma \sim 0.83$ for the free convection layer. The value of γ stays surprisingly constant up to 0.5 Z_i, indicating that the $Z^{-4/3}$ decrease in the inertial subrange intensity continues well above 0.1 Z_i (see C_T^2 plot in Fig. 7). The variation of $N \varepsilon^{-1/3}$ above 0.1 Z_i, non-dimensionalized with mixed layer parameters, θ_* and Z_i is shown in Fig. (11) and can be approximated as follows:

$$\frac{N \varepsilon^{-1/3}}{\theta_*^2 Z_i^{-4/3}} = \begin{cases} 0.83 (Z/Z_i)^{-4/3} & ; \; Z \leq 0.5 Z_i \\ 2.1 & ; \; 0.5 Z_i \leq Z \leq 0.7 Z_i \\ 6.1 (Z/Z_i)^3 & ; \; 0.7 Z_i \leq Z \leq Z_i \end{cases} \qquad (12)$$

This behaviour of the temperature spectrum agrees qualitatively with the ε and N profiles presented by Caughey and Rayment (1974).

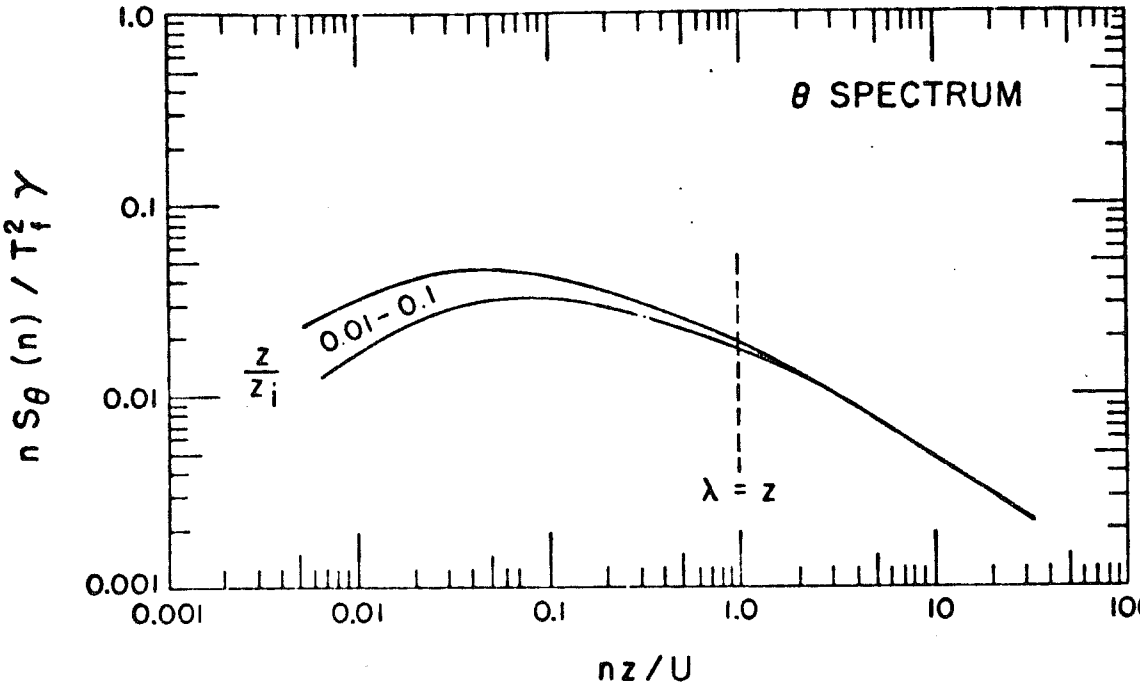

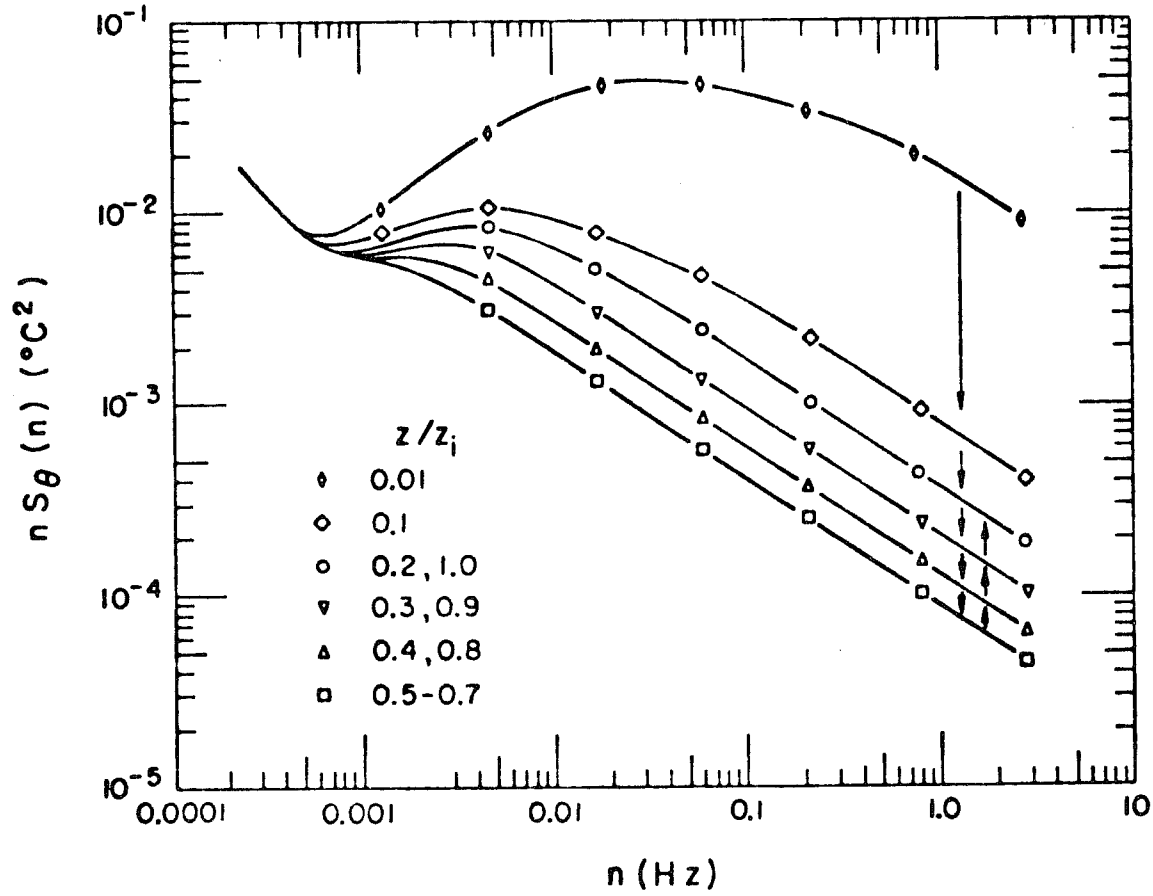

Fig. 7: Universal curve for the θ spectrum (upper figure) in the range 0.01 z_i < z <0.1 z_i. T_f^* is the free convection scaling temperature and represents the dimensionless grouping, $N\varepsilon^{-\frac{1}{3}} / Q_0^{4/3} (g/T)^{-\frac{2}{3}} z^{-4/3}$ which is a constant (~0.33) in this height range. Idealized temperature spectra in dimensional coordinates (lower figure) show the variation in spectral behaviour with z/z_i.

The above empirical relationship can be used to collapse all inertial subrange temperature spectra into a single curve in a plot similar to Fig. 5. Here the dimensionless ratio of (12) plays the same role as 2/3 in Eq. (4). Bringing the inertial subrange Θ spectra together in this manner causes the low frequency end to spread out, but no systematic trend emerges in the composite plots because of run-to-run variations in the details of their low frequency behaviour.

It seems clear that the increase in inertial subrange variance above .7 z_i is a direct consequence of mixing produced by the entrainment of warm air from the inversion into the boundary layer. The temperature and heat flux traces in Fig. (8) provide clear evidence of such entrainment. Only portions of the $\overline{w\theta}$ traces where significant heat flux exists are shown and these regions are shaded to distinguish them from temperature traces. The regions of upward heat flux are thermals which originate near the surface layer. The regions of downward heat flux appear between the tops of the thermals, and these are also characterized by positive bursts in the temperature trace. The structure of the bursts suggests that the entraining warm air descends in the form of discrete plumes. Further evidence for this interpretation comes from recent acoustic sounder results obtained at Cardington. Figure (9) shows a strong subsidence inversion perturbed by convective elements, the regions of entrained air descending into the boundary layer are clearly visible.

The entrainment mechanism has been studied in some detail by Rayment and Readings (1974). They observed small rolls on the convective hummocks which eventually 'broke' and resulted in the transfer of warm air across the inversion interface (Fig. 10). Whether this mechanism is generally applicable must await a further series of multilevel measurements, preferably in association with remote techniques.

2.3 Variances and Structure Parameters

As mentioned earlier the free convection predictions for the peak wavelengths in W and Θ spectra are valid to $\simeq$ 0.1 z_i.

The asymptotic predictions for $\overline{w^2}$ and $\overline{\theta^2}$ expressed in surface layer parameters (Wyngaard et. al. 1971a) are

$$\overline{w^2}/u_*^2 \approx 3.6\,(-z/L)^{2/3} \qquad (13)$$

$$\overline{\theta^2}/T_*^2 \approx 0.9\,(-z/L)^{-2/3} \qquad (14)$$

These expressions convert directly to mixed layer parameters with only a change in the value of the constant. Thus, we have, replacing equations (13) and (14),

$$\overline{w^2}/w_*^2 \approx 1.8\,(z/z_i)^{2/3} \qquad (15)$$

$$\overline{\theta^2}/\theta_*^2 \approx 1.8\,(z/z_i)^{-2/3} \qquad (16)$$

These predictions are shown as dashed lines in Fig. 11 and form a reasonable fit to the data to a height of about 0.1 z_i. Above this level the data exhibits more scatter than is apparent at the lower levels.

Comparing the Minnesota W variance data above 0.1 z_i with aircraft, water tank and numerical model results (surveyed by Deardorff and Willis, 1974) one finds the aircraft results fall within the scatter of the present data points. The magnitudes in the tank and numerical experiments tend to be slightly greater than the atmospheric measurements. As for the height of the maximum variance the tank data show a peak around 0.5 z_i - as in the aircraft data and barely suggested in the Minnesota data - while the numerical data show a peak somewhat lower. The most significant departure from the tank and numerical results is the absence of any marked drop in W variance near the inversion base.

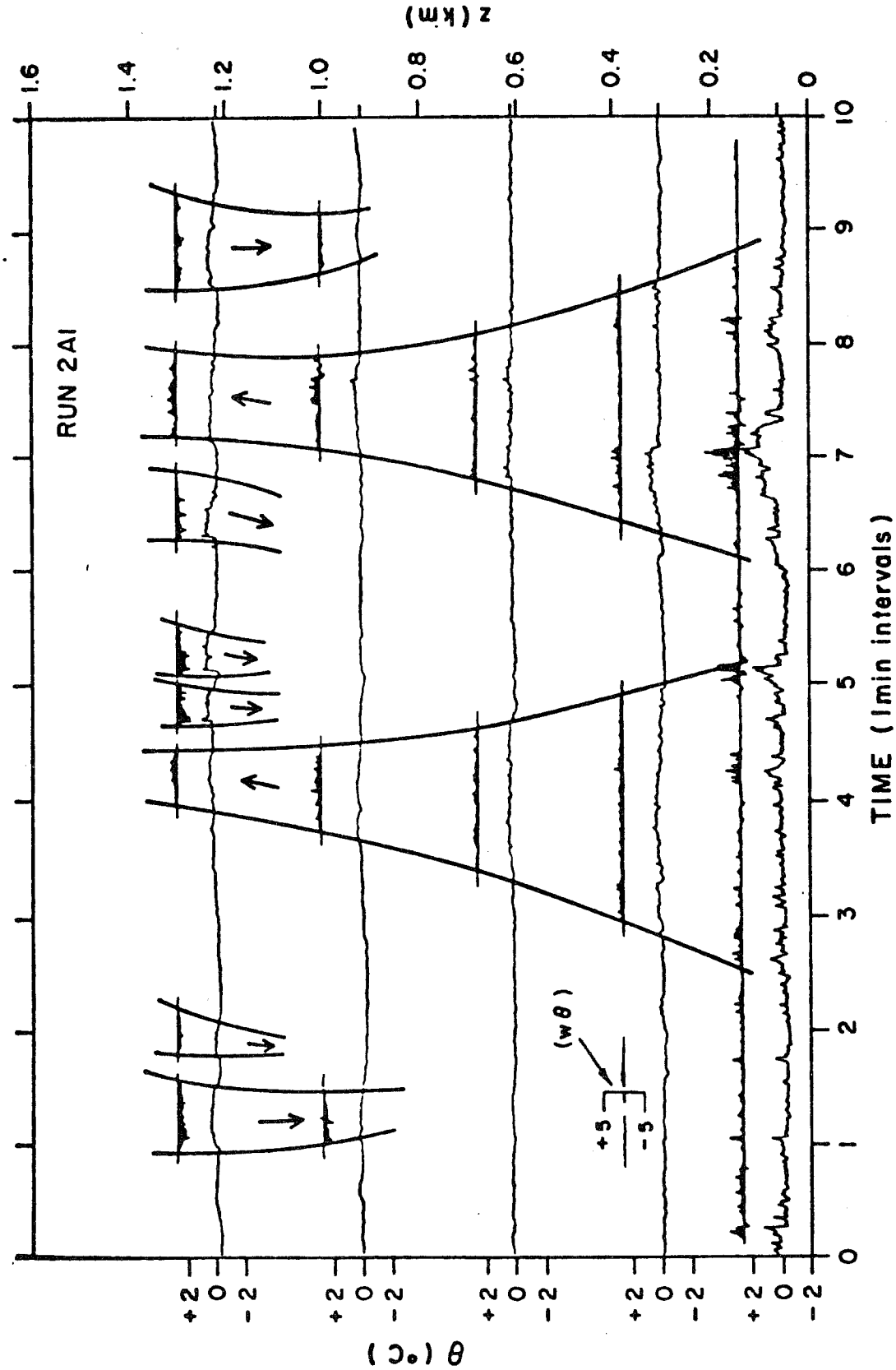

Figure 8: Temperature fluctuations observed during the 10-min.period from 1321 to 1331 towards the end of run 2A1. The top of the figure represents the inversion base for this period. The magnitude and direction of the instantaneous vertical heat flux for the top level are indicated by the shaded fluctuations traced above it.

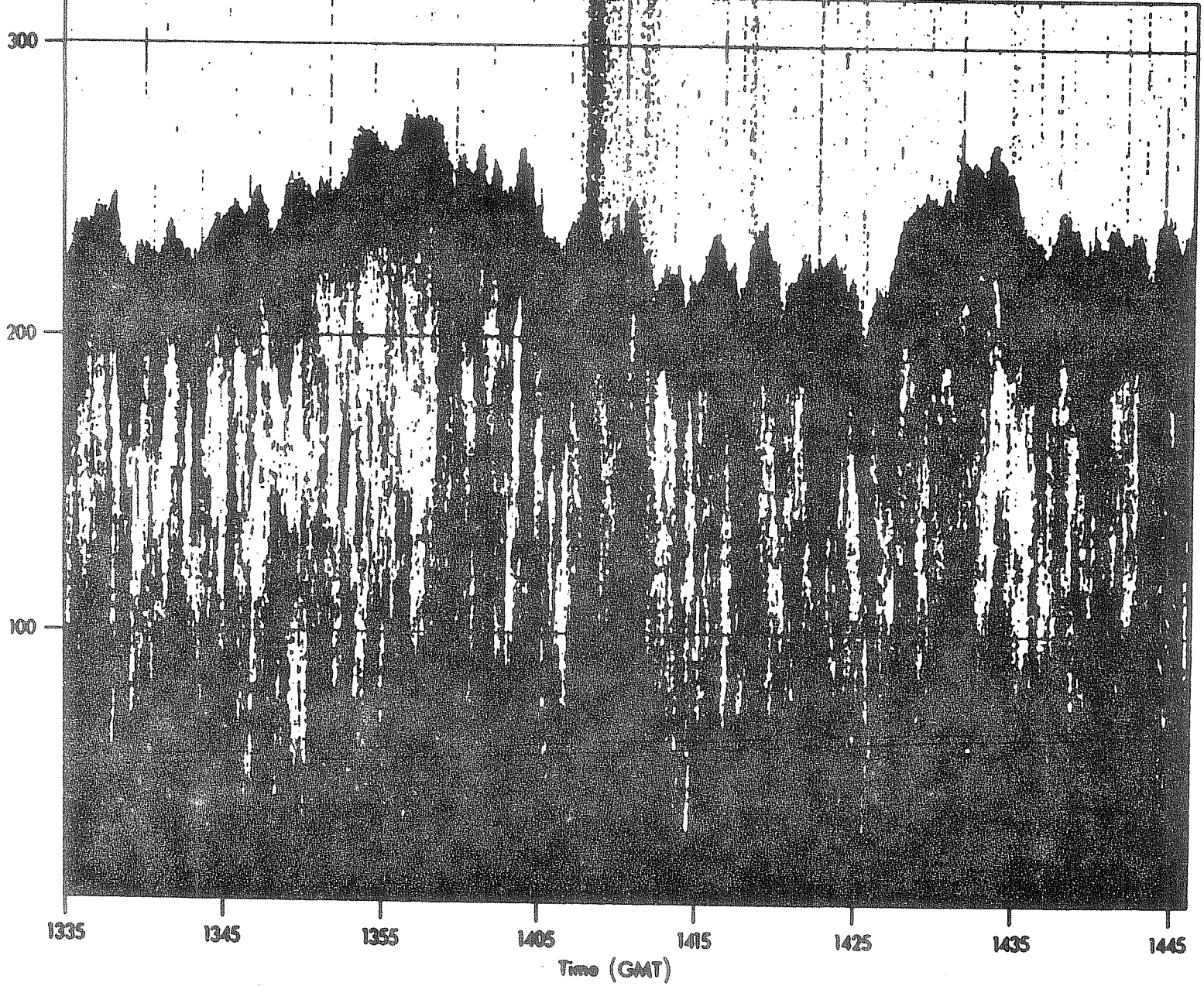

Figure 9: Acoustic sounder record showing the interaction of thermal plumes with intense ($10^{o}C$) subsidence inversion (base at 200 m).

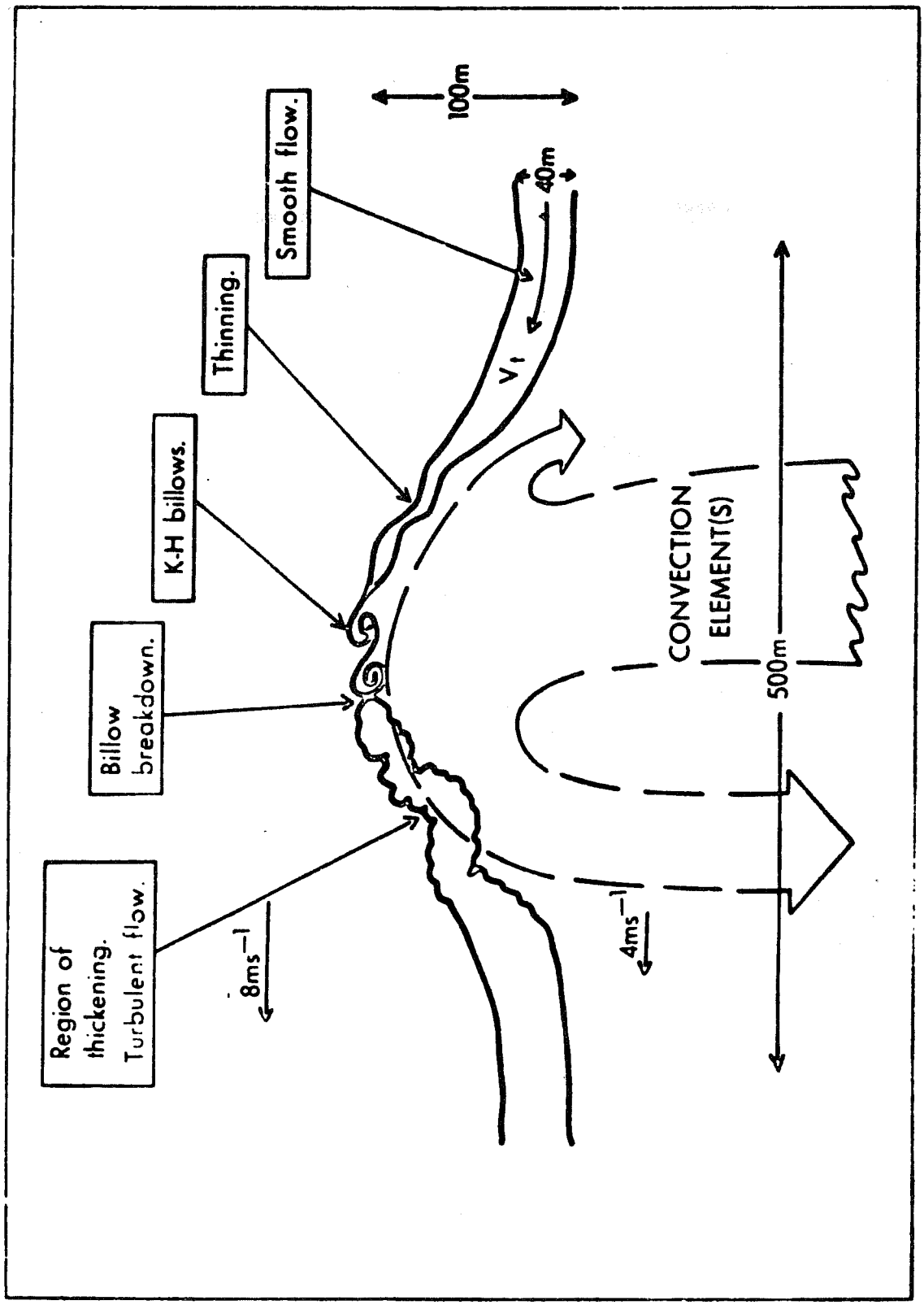

Figure 10: Schematic diagram of the entrainment process at the top of the convective boundary layer.

This is consistent with the spectral behaviour observed in Fig. (5) showing no appreciable change in spectral intensity or shape above 0.1 z_i and probably reflects the different upper boundary conditions that exist in the atmosphere compared to the experiments.

The Θ variance above 0.1 z_i shows a steeper decrease with height than predicted by local free-convection similarity. The decrease continues to 0.5 z_i, where it reaches a minimum value. Above 0.5 z_i, the variance increases with height, clearly the result of mixing produced by entrainment of warm air into the boundary layer through the inversion.

The structure parameters, C_V^2 and C_T^2 reflect the inertial subrange behaviour in the velocity and temperature spectra respectively. Their chief application is to studies of wave propagation in the atmosphere. The expression for C_V^2, analogous to the one for C_T^2 is (Kaimal, 1973)

$$C_V^2 = 4\alpha_1 \varepsilon^{2/3} \approx 2\varepsilon^{2/3} \tag{17}$$

The asymptotic surface layer prediction for C_V^2 derived from the surface layer relationship (Wyngaard and Coté, 1971) gives

$$\frac{C_V^2 z_i^{2/3}}{w_*^2} = \text{constant} \tag{18}$$

which is unity for the Kansas data but higher for the Minnesota data. A useful approximation for the dimensionless C_V^2 in the range $0.01\ z_i \leq z \leq 0.1\ z_i$ is,

$$\frac{C_V^2 z^{2/3}}{w_*^2} = 1.3 + 0.1\left(z/z_i\right)^{-2/3} \tag{19}$$

The C_T^2 measurements provide, by far, the best agreement to the Kansas free-convection predictions in the lower half of the boundary layer, with considerably less scatter than any other parameter considered. From Eq's (10) and 12) we find,

$$\frac{C_T^2 z^{2/3}}{\theta_*^2} = 2.67\left(z/z_i\right)^{-4/3} \tag{20}$$

which is indicated by the dashed line in Fig. (11). These results are in agreement with Tsvang's (1969) observations that showed the -4/3 power law extending to heights of order 500 m. The trend stops at 0.5 z_i and begins to increase with height above 0.7 z_i, once more reflecting the mixing produced by warm air entraining into the boundary layer.

3. Stable Conditions

In stable conditions the atmosphere can support wave motion and this coexistence of waves and turbulence complicates the investigation of the turbulence characteristics Shown in Fig. (12) is a somewhat typical acoustic sounder record taken during stable conditions. Well defined 'wave like' features are present and the patchy nature of the turbulence activity is clearly illustrated. Atmospheric spectra recorded in such conditions show a double peaked character, with evidence of a spectral 'gap' (or minimum) at intermediate frequencies (approx. 10^{-2} Hz). To proceed with the classification/understanding of the turbulence spectra obtained in such conditions it is obviously necessary to remove the contributions (at low frequency) arising from the oscillations in the time series. This is possible provided the major fluctuations from turbulence and waves fall in different frequency bands. In the surface layer this is generally the case (Caughey, 1976) but at the higher levels the spectral gap closes, so that by about 100 m height the spectrum assumes an almost single peaked character, Fig. (13). Results indicate that the peak at low frequency falls in the neighbourhood of the Brunt-Viasala frequency.

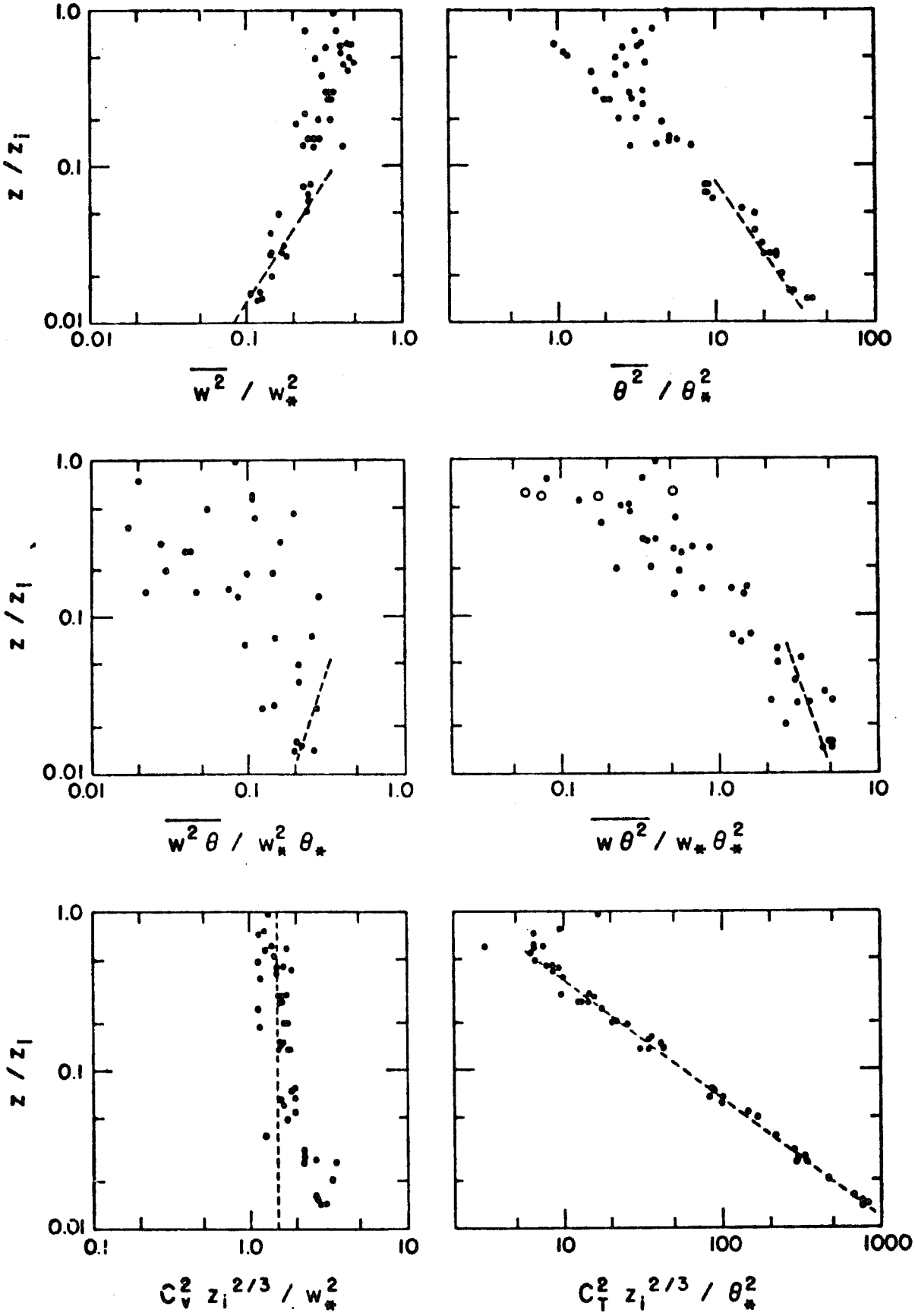

Figure 11: Vertical profiles of higher-order moments and structure functions. The dashed lines are free convection prediction based on the Kansas data.

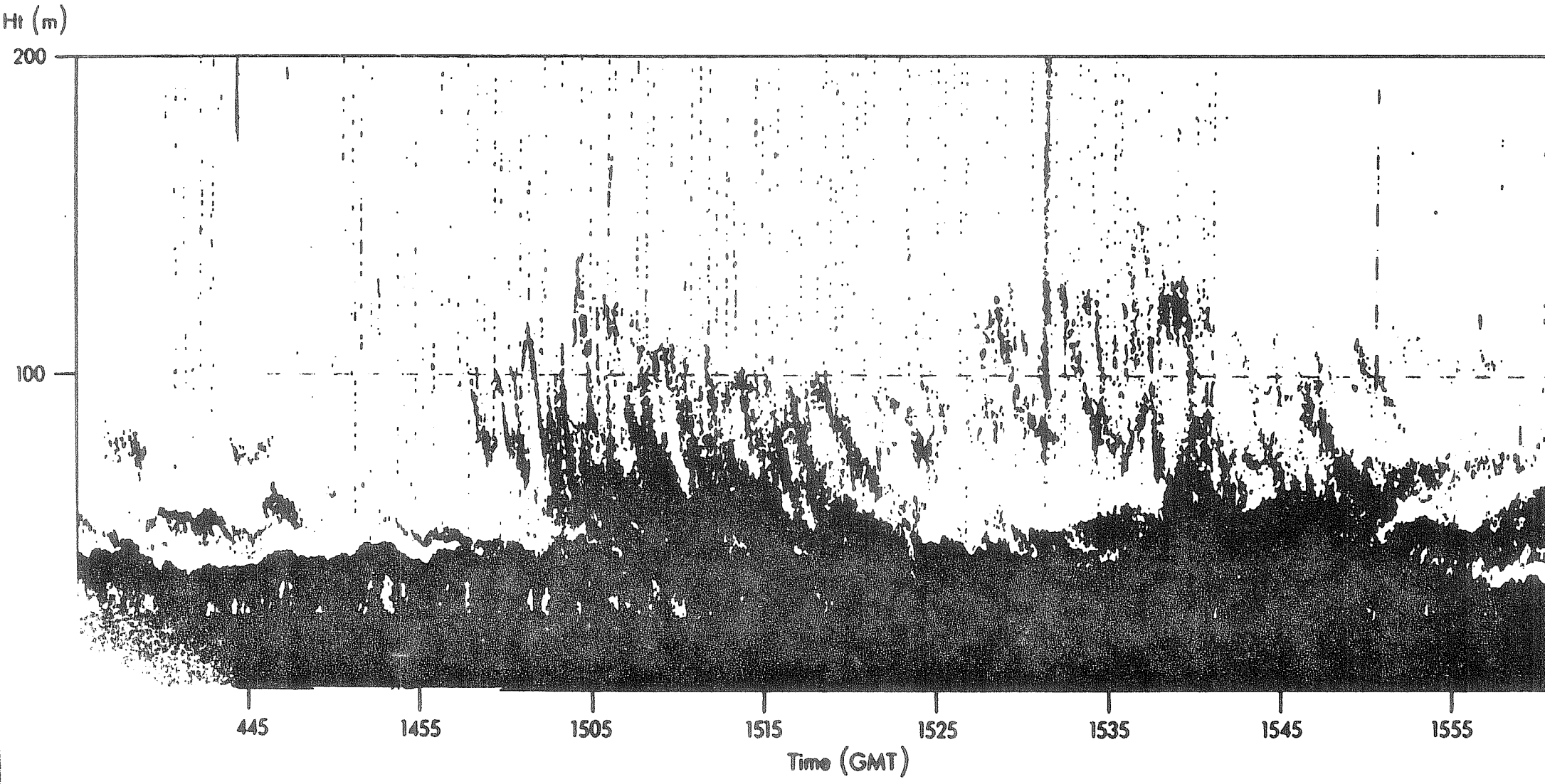

Fig 12

Acoustic sounder record showing the presence of internal waves

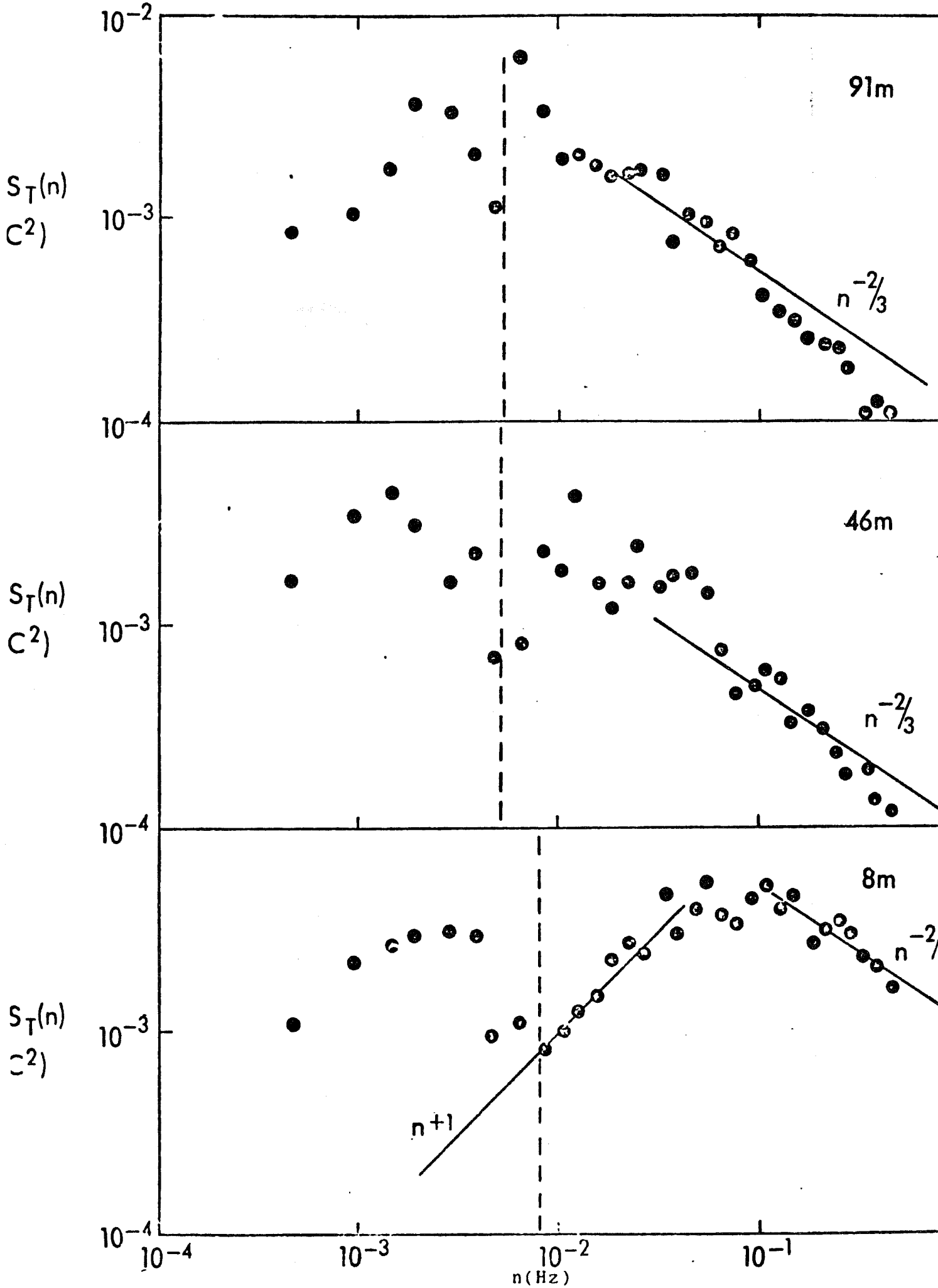

Figure 13: Temperature spectra at 8,46 and 91 m illustrating the movement of the turbulence subrange to lower frequencies and the narrowing

By integrating over frequencies greater than a chosen 'cut-off' value Kaimal (1973) computed variances/covariances relevant to the turbulence subrange alone. When presented in the non-dimensional form all spectra and cospectra were found to collapse into a set of universal curves. These curves have been found applicable to spectra recorded over the Cardington site, which is considerably less ideal than that in Kansas, Figs. (14) and (15). The behaviour of the scaling parameter $(f)_{u,T}$ with Richardson number was also in agreement with the findings of Kaimal (1973). This approach may offer a way for describing the characteristics of atmospheric spectra in stable boundary layers at heights less than the upper limit of the nocturnal inversion.

Conclusions:

The main points from the results described in this paper may be summarised as follows :

1. Convective conditions,

(a) The spectra of velocity components in the boundary layer can be generalised within the framework of mixed layer similarity. With appropriate normalization, the W spectrum can be reduced to a family of curves which spreads out as a function of Z/Z_i at low frequencies, but converge to a single universal curve in the inertial subrange. The U and V spectra generalised in the same manner show universal behaviour, but without the Z/Z_i dependence apparent in W. The onset of the inertial subrange in the mixed layer occurs at a wavelength $\lambda \approx 0.1\ Z_i$

(b) The temperature spectra above $0.1\ Z_i$ cannot be generalised in the same manner as the velocity spectra because of the variability in the low frequency behaviour. However, the inertial subrange level is more predictable decreasing as $(Z/Z_i)^{-4/3}$ up to $0.5\ Z_i$ and increasing as $(Z/Z_i)^3$ above $0.7\ Z_i$. Below $0.1\ Z_i$ they behave much like surface layer spectra.

(c) The characteristic wavelength, λ_m, for W and Θ increases linearly with Z in the height range $\sim L \rightarrow 0.1\ Z_i$ following free convection prediction, but levels off to a nearly constant value ($\lambda_m \sim 1.5\ Z_i$) above that height. λ_m for U and V stays approximately the same ($\approx 1.5\ Z_i$) throughout the depth of the boundary layer.

(d) The wavelength $\lambda_m \approx 1.5\ Z_i$, observed in the velocity and temperature spectra, corresponds to the length scale of large thermals that appear to dominate the circulation in the boundary layer.

(e) There is evidence of substantial heat entrainment into the boundary layer through the capping inversion. The entrained warm air descends in the form of 'inverted plumes' strongly affecting the temperature and heat flux statistics in the upper half of the boundary layer.

(f) Free convection predictions for the variances of W and Θ also appear to be valid to a height of $0.1\ Z_i$. The triple moments indicate a much shallower free-convection layer but this may be the result of inadequate averaging time. C_v^2 reaches its real constant value only above $0.1\ Z_i$, while C_T^2 fits the prediction to a height of $0.5\ Z_i$.

2. Stable conditions,

(a) In the first few tens of metres the power and co-spectra can be generalised and described in terms of the Richardson number when the low frequency contributions arising from waves etc., have been removed.

(b) At higher levels the fluctuations arising from wave motion and turbulence begin to overlap in frequency and this increases the difficulty in isolating a turbulence subrange.

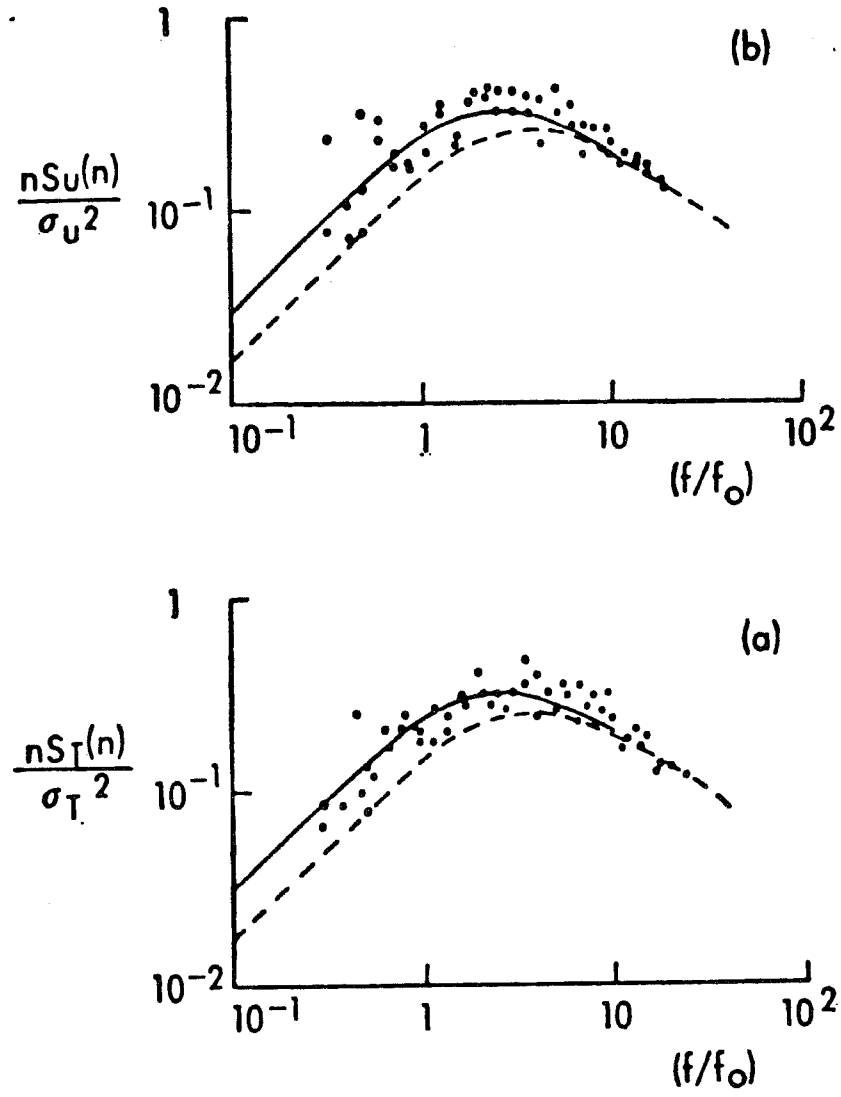

Fig. 14: Non-dimensional temperature and horizontal wind speed spectra at 8 m for two runs on the 8/9 November 1972 plotted versus f/f_o, compared with the universal curve given by Kaimal (1973)

$$\frac{n\,S_\alpha(n)}{\alpha^2} = \frac{A\,(f/f_o)}{1 + A\,(f/f_o)^{5/3}}$$

α = u, T

A = .3, ———

A = .16, - - - - - - - -

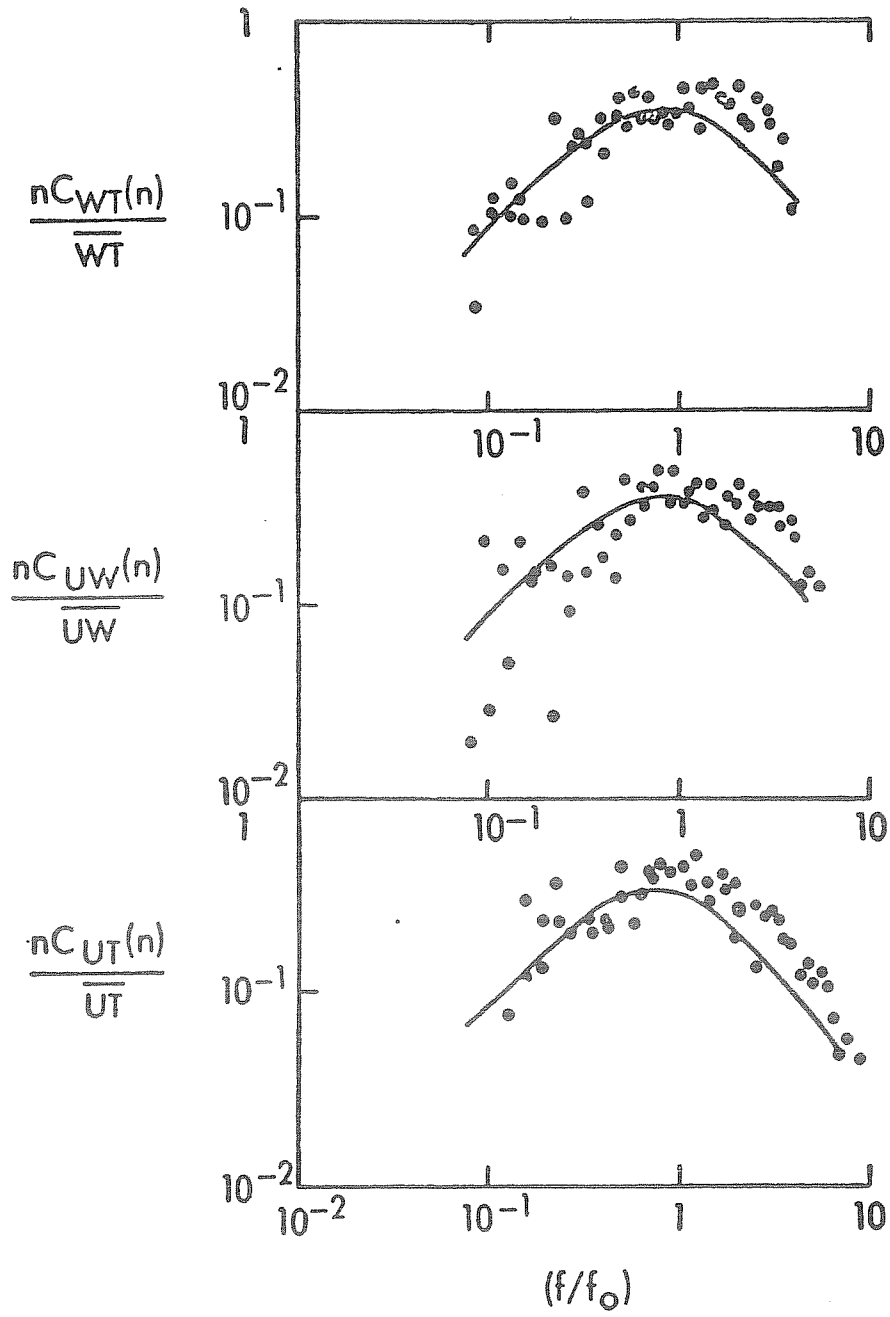

Fig. 15: Non-dimensional cospectra plotted versus f/f_o , compared to the universal curves from Kaimal (1973).

$$\frac{n\,S_{\alpha\beta}(n)}{\overline{\alpha\beta}} = \frac{0.88\,(f/f_o)}{1 + 1.5\,(f/f_o)^{2.1}}$$

$$\overline{\alpha\beta} = \overline{w\theta}\,,\ \overline{uw}$$

$$\frac{n\,S_{\alpha\beta}(n)}{\overline{\alpha\beta}} = \frac{0.85\,(f/f_o)}{1 + 1.7\,(f/f_o)^{2.2}}$$

$$\overline{\alpha\beta} = \overline{u\theta}$$

List of Symbols

$\bar{u}$	- mean wind speed
U,V,W	- fluctuating wind components in the longitudinal, lateral and vertical directions.
T	- mean temperature
θ	- fluctuating temperature
ρ	- air density
τ_o	- surface shear stress ($\approx -\rho \overline{uw}$, 4m)
Q	- vertical temperature flux ($= \overline{w\theta}$)
Q_o	- surface temperature flux ($\approx \overline{w\theta}$, 4m)
g/T	- buoyancy parameter
ε	- dissipation rate of turbulent kinetic energy
k	- von Karman's constant
Ψ	- dimensionless dissipation rate $\varepsilon T/g Q_o$
N	- dissipation rate for half the temperature variance
δ	- a dimensionless structure parameter, $N\varepsilon^{-1/3}/Q_o^{4/3}(g/T)^{-2/3} z^{-4/3}$
α_1	- spectral constant for 1-dimensional U spectra (~ 0.5)
β_1	- spectral constant for the 1-dimensional θ spectra (~ 0.8)
z	- height above ground
z_i	- height of the lowest inversion base
L	- Monin-Obukhov length
n	- cyclic frequency
n_m	- frequency of the logarithmic spectral peak
λ_m	- wavelength corresponding to n_m ($= \bar{u}/n_m$)
f	- dimensionless frequency $nz/\bar{u}$
f_i	- dimensionless frequency $nz_i/\bar{u}$
C_T^2	- structure parameter for temperature
C_V^2	- structure parameter for velocity
U_*, T_*	- scaling velocity and temperature for the surface shear layer
U_f, T_f	- scaling velocity and temperature for the free-convection layer

$w_*\theta_*$ - scaling velocity and temperature for the mixed layer

$(f_o)_{u,T}$ - the intercept on a reduced frequency scale ($f = n z/\bar{u}$) at which the extrapolated inertial subrange slope meets the line $\frac{n S_\alpha(n)}{\sigma^2} = 1$, for α = U and T.

Peferences:

Busch, N E 1973 — The Surface Boundary Layer. Bound. Layer Meteor. 4, 213 - 240.

Businger, J A, J.C.Wyngaard, Y Izumi and E F Bradley, 1971 — Flux Profile relationships in the atmospheric surface layer. J. Atmos. Sci., 28, 181 - 189.

Caughey, S J and R Rayment, 1974 — High frequency temperature fluctuations in the atmospheric boundary layer. Bound. Layer Meteor. 5, 489 - 503.

Caughey, S J and C J Readings, 1974 — The Vertical Component of Turbulence in convective conditions. Advances in Geophysics, Vol. 18A, 125 - 130.

Caughey, S J and C J Readings, 1975 — Turbulent fluctuations in convective conditions. Quart. J. R. Met. Soc. 101, 537 - 542.

Caughey, S J, 1976 — Boundary Layer turbulence spectra in stable conditions. Bound. Layer Meteor. (in press).

Clarke, R H and Hess, G D, 1973 — 'On the appropriate scaling for velocity and temperature in the planetary boundary layer'. J. Atmos. Sci., 30, 1346 - 1353.

Deardorff, J W, 1972 — Numerical investigation of neutral and unstable planetary boundary layers. J. Atmos. Sci., 29, 91 - 115.

Deardorff, J W and G E Willis, 1974 — Computer and laboratory modelling of the vertical diffusion of non-buoyant particles in the mixed layer. Advances in Geophysics, 18B, 187 - 200.

Deardorff, J W, 1974 (a) — Three-dimensional numerical study of the height and the mean structure of a heated planetary boundary layer. Boundary Layer Met., 7, 81 - 106.

Deardorff, J W, 1974 (b) — Three-dimensional numerical study of turbulence in an entraining mixed layer. Bound. Layer Meteorol., 7, 199 - 226.

Frisch, A S, R B Chadwick, W R Moninger and J M Young, 1975 — Observation of boundary layer convection cells measured by dual-Doppler radar and echo-sounder and by micro-barograph array. Bound. Layer Meteor. 3, 199 - 226.

Hardy, K R and J Ottersten, 1969 — Radar investigation of convective patterns in the clear atmosphere. J. Atmos. Sci. 26, 666-672.

Haugen, D A, Kaimal, J C, Readings C J and Rayment R, 1975 — 'A comparison of balloon-borne and tower-mounted instrumentation for probing the atmospheric boundary layer'. J. Appl. Met., 14, 540 - 545.

Izumi, Y and S J Caughey, 1976 — 'Minnesota 1973 atmospheric boundary layer experiment data report'. AFCRL Research Report No. 547.

Kaimal, J C, 1973 — 'Turbulence spectra, length scales and structure parameters in the stable surface layer'. Bound.Layer Meteor., 4, 289 - 309.

Kaimal, J C, Wyngaard, J C Y Izumi and O R Coté, 1972 — 'Spectral characteristics of surface layer turbulence'. Quart. J. R. Met. Soc. 98, 563 - 589.

Kaimal, J C, Wyngaard, J C, D A Haugen, O R Coté, Y Izumi, S J Caughey and C J Readings, 1976 — 'Turbulence Structure in the convective boundary layer'. To be published in J. Atmos. Sci.

Konrad, T G, 1970 — 'The dynamics of the convective process in clear air as seen by radar'. J. Atmos. Sci., 27, 1138 - 1147.

Kukharets, V P, 1974 — 'Spectra of the vertical wind component in the atmospheric boundary layer'. Izv. Atmos. and Ocean Phys. 10, 375 - 378. (English ed.).

Rayment, R and C J Readings, 1974 — 'A case study of the structure and energetics of an inversion'. Quart. J. R. Met. Soc., 100, 221-233.

Rowland, J R and A Arnold, 1975 — 'Vertical velocity structure and geometry,of clear air convection elements'. Preprints of the 16th Radar Meteorology Conference (American Meteorological Society) 296 - 303.

Tennekes, H, 1975 — 'Reply to comments on "A model for the dynamics of the inversion above a convective boundary layer",'. J. Atmos. Sci., 32, 992-995.

Tsvang, L R, 1969 — 'Microstructure of temperature fields in the free atmosphere.' Radio Sci., 1175 - 1177.

Wyngaard, J C and O R Coté, 1971 — 'The budgets of turbulent kinetic energy and temperature variance in the atmospheric surface layer'. J. Atmos. Sci., 28, 190 - 201.

Wyngaard, J C, O R Coté, and Y Izumi, 1971 — 'Local free convection, similarity, and the budgets of shear stress and heat flux'. J. Atmos. Sci., 28, 1171 - 1182.

Wyngaard, J C, O R Coté and K S Rao, 1974 — 'Modelling the atmospheric boundary layer'. Adv.Geophys. 18A, 193 - 212.

Zilitinkevich, S S, 1972 — 'On the determination of the height of the Ekman boundary layer'. Bound. Layer Met. , 3 , 141 - 145.